A Deterministic Approach for Designing Conditionally Stable Amplifiers

Marion Lee Edwards, *Senior Member, IEEE*, Sheng Cheng, *Member, IEEE*, and Jeffrey H. Sinsky, *Member, IEEE*

Abstract—**Microwave devices with the Rollet parameter *(k)* less than one can always be made stable by resistive loading. In cases where noise figure or output power is at a premium, the performance of an amplifier can often be enhanced by using a design where *k* is less than unity thereby avoiding resistive loading. While a simultaneous conjugate match is impossible for such conditionally stable designs, single-sided matching can be achieved. Low-noise and power designs are examples where single-sided matching considerations naturally occur. With single-sided matching and $0 < k < 1$, a design method is presented that results in device impedances on both the matched and unmatched sides that are always inside the Unit Smith Chart. This condition is referred to as jointly (input/output) stable. Gains resulting from jointly stable terminating impedances are shown to be bounded, the upper bound being given by $2 \cdot k \cdot$ maximum stable gain. The design on an output-matched, conditionally stable amplifier is illustrated.**

I. Introduction

FOR high-performance amplifier applications, it is often desirable not to stabilize potentially unstable devices if the source and load impedances are well controlled. A design technique that permits the use of k less than one thereby avoids resistive loading (otherwise used to make k greater than one) and helps achieve better noise figure and output power. Unfortunately, the design of conditionally stable amplifiers may not be a straight forward process as illustrated in the MESFET example shown in Fig. 1.

Here the designer selected a stable source reflection coefficient Γ_S (based on noise or other considerations), designed an appropriate input matching network (IMN) to transform 50 Ω into Γ_S, and now wishes the output to be matched. With the IMN connected to the FET gate, an output reflection coefficient Γ_{OUT} is observed looking into the drain. An output matching network (OMN) now needs to be designed to transform 50 Ω to Γ^*_{OUT} so that the drain will see a conjugately matched load. Unfortunately, as seen in the figure, this can result in a Γ_L located on the unstable side of the load stability circle. At this point, the designer has several choices: 1) continue the design of the OMN accepting the location of Γ^*_{OUT}, 2) design an OMN that results in a Γ_L that is near Γ^*_{OUT} but on the stable side of the load stability circle, and accept an unknown degraded match at the output of the circuit [1], or 3) restart the design changing Γ_S hoping that the new resulting Γ^*_{OUT} will fall in the stable region of the load plane [2]. In choice 1), the output is conjugately matched, but because of the location of Γ_L the input is unstable, i.e. referring to (1) and (3), $|\Gamma_{\mathrm{IN}}(\Gamma^*_{\mathrm{OUT}}(\Gamma_S))| > 1$. In this case the input impedance will have a negative real part and with the "proper" source termination could support oscillations. In choices 2) and 3), the design process becomes uncertain and requires "trial and error" iterations to complete the design.

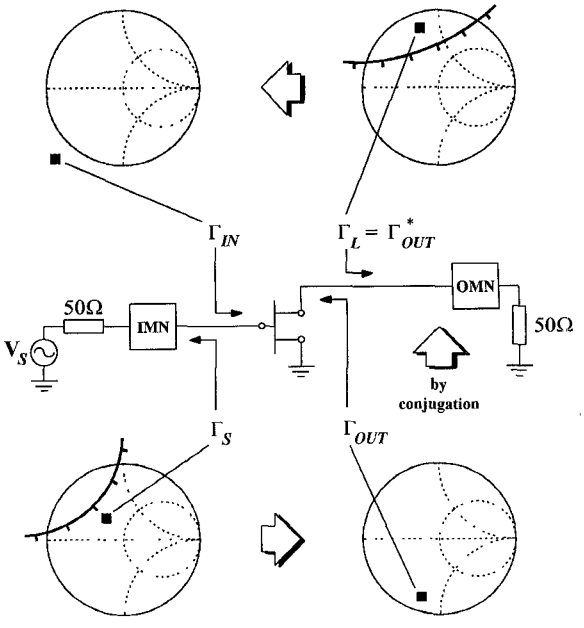

Fig. 1. Illustration of the stability problem in designing a conditionally stable amplifier. Tick marks designate stableside of stability circles.

The above example illustrates that a circuit can be output stable, $|\Gamma_{\mathrm{OUT}}| < 1$, but input unstable, $|\Gamma_{\mathrm{IN}}| > 1$, conditions manifested by examining the source and load stability circles, respectively. Output matched circuits for which $|\Gamma_{\mathrm{OUT}}(\Gamma_S)| < 1$ and $|\Gamma_{\mathrm{IN}}(\Gamma^*_{\mathrm{OUT}}(\Gamma_S))| < 1$ are said to be jointly stable. A non-iterative process to design a jointly stable output matched circuit would be possible if the stable region in the load plane (Fig. 1—upper right) were mapped onto the Γ_S-plane. This mapped region in the Γ_S-plane will be either a disk (region inside of a circle) or a disk complement (region outside of a circle) since the reflection coefficients are related by linear fractional (or bilinear) transformations [3], i.e., (1)–(4) [1]–[4]. An exact knowledge of this region in the Γ_S-plane would permit a designer to select source impedances with an *a priori* knowledge that the matched load will be located on the stable side of the load stability circle

$$\Gamma_{\mathrm{IN}} = f(\Gamma_L) = \frac{S_{11} - \Delta\Gamma_L}{1 - S_{22}\Gamma_L} \tag{1}$$

Manuscript received September 14, 1994; revised January 12, 1995.

The authors are with the Applied Physics Laboratory and Whiting School of Engineering, Johns Hopkins University, Laurel, MD USA.

IEEE Log Number 9412048.

$$\Gamma_L = f^{-1}(\Gamma_{IN}) = \frac{S_{11} - \Gamma_{IN}}{\Delta - S_{22}\Gamma_{IN}} \tag{2}$$

$$\Gamma_{OUT} = g(\Gamma_S) = \frac{S_{22} - \Delta\Gamma_S}{1 - S_{11}\Gamma_S} \tag{3}$$

$$\Gamma_S = g^{-1}(\Gamma_{OUT}) = \frac{S_{22} - \Gamma_{OUT}}{\Delta - S_{11}\Gamma_{OUT}} \tag{4}$$

where

$$\Delta = S_{11}S_{22} - S_{12}S_{21}. \tag{5}$$

II. Background

To facilitate the theoretical development, the following algebraic combinations of S-parameters are defined [1]

$$B_1 = D_1 + E_1 \tag{6}$$

$$C_1 = S_{11} - \Delta S_{22}^* \tag{7}$$

$$D_1 = |S_{11}|^2 - |\Delta|^2 \tag{8}$$

$$E_1 = 1 - |S_{22}|^2 \tag{9}$$

$$k = \frac{E_1 - D_1}{2|S_{12}S_{21}|}. \tag{10}$$

Additionally, the following easily verified relationship turns out to be useful

$$|C_1|^2 = |S_{12}S_{21}|^2 + D_1E_1. \tag{11}$$

The conventional stable region [2] in the source plane, whose boundary is the source stability circle, is here referred to as the *output stable region in the source plane* since it defines the Γ_S values that result in $|\Gamma_{OUT}(\Gamma_S)| < 1$. Using (3), this results in region which is either a disk or disk complement. In either case the boundary is the circle with radius, r_S, and center, C_S, given by

$$r_S = \left|\frac{S_{12}S_{21}}{D_1}\right| \tag{12a}$$

$$C_S = \frac{C_1^*}{D_1}. \tag{12b}$$

If $D_1 < 0$ [3] then the stable region is the "disk," $|\Gamma_S - C_S| < r_S$, whereas, if $D_1 > 0$ then the stable region is the "disk complement," $|\Gamma_S - C_S| > r_S$. Since D_1 is a real number the angular direction of the center, C_S, is determined only by the angle of the complex number C_1^*. To emphasize this dependency the center of the stability circle is represented as the product of a scalar and a unit vector in the complex plane, i.e., $C_S = c_S\hat{c}_S$, where

$$c_S = \frac{|C_1|}{D_1} \quad \text{and} \quad \hat{c}_S = \frac{C_1^*}{|C_1|}. \tag{13}$$

Fig. 2 illustrates the eight different topological relationships that the conventional stability regions can have with the Unit Smith Chart where Fig. 2(a) and 2(h) illustrates unconditionally stable circuits, i.e., the USC is contained in the stable region, while Fig. 2(d) and 2(e) illustrates absolutely unstable circuits. This paper focuses on conditionally stable circuits exemplified by Fig. 2(b) and 2(f), which will be shown in the next section to be equivalent to $|k| < 1$.

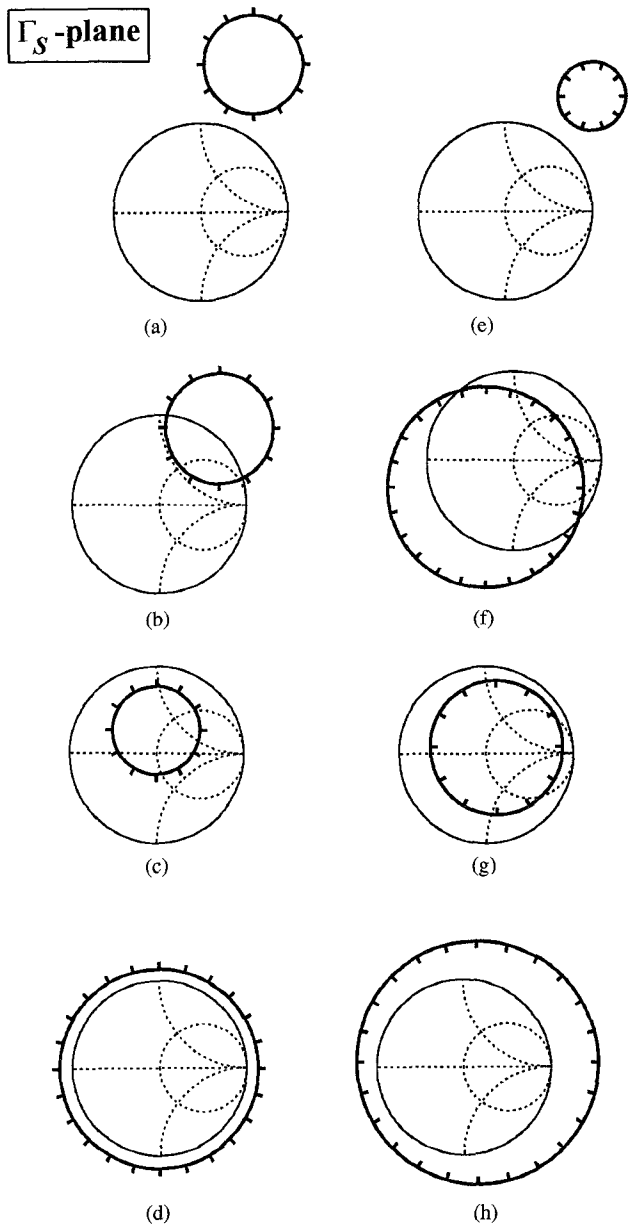

Fig. 2. Stability circle configurations. $D_1 > 0$ for (a)–(d), and $D_1 < 0$ for (e)–(h).

III. Geometric Implication of $|k| < 1$

In this section it is shown that $-1 < k < 1$ occurs if and only if the stability circle intersects the unit circle, i.e., when the stability circle radius is strictly between the following two limits:

$$||C_S| - 1| < r_S < |C_S| + 1. \tag{14}$$

The left inequality in (14) implies that

$$1 + |C_S|^2 - r_S^2 < 2|C_S|$$

and using (12a), (12b), and (11) one can obtain

$$\frac{D_1 + E_1}{D_1} < 2|C_S|. \tag{15}$$

Similarly, the right side of (14) implies

$$-2|C_S| < \frac{D_1 + E_1}{D_1} \tag{16}$$

and by virtue of (15) and (16)

$$\left|\frac{D_1 + E_1}{D_1}\right| < 2|C_S|.$$

Since both sides are positive, this relationship can be squared preserving the inequality. Using (12b) it follows that

$$(D_1 + E_1)^2 < 4|C_1|^2. \tag{17}$$

Substituting for $|C_1|^2$ using (11) and applying (10) results in

$$k^2 = \left(\frac{E_1 - D_1}{2|S_{12}S_{21}|}\right)^2 < 1$$

$$or\ |k| < 1.$$

The above argument is reversible in that $|k| < 1$ implies that either $r_S > ||C_S| - 1|$ or $r_S < |C_S| + 1$ and therefore, the stability circle intersects the unit circle.

IV. Gain Properties for $|k| < 1$ (Invariant Points and Monotonicity)

It is now shown that when $|k| < 1$ the stability circle and the unit circle intersect in two distinct points. Using the approach of Collins [4] these two points are shown to be common to all the available gain circles and therefore called invariant points. The geometric relationships between the stability circle, the gain circle, and the unit circle can then be determined solely by comparing the centers of the circles. This property will become useful when the gain associated with input stable region in the source plane is discussed in a later section. The geometry together with the monotonic nature of the gain and its singularity near a stability circle will be used in establishing when the gain is constrained by an upper bound.

The source stability circle is found by squaring $|\Gamma_{\text{OUT}}| = 1$ and substituting (3) to get

$$|1 - S_{11}\Gamma_S|^2 - |S_{22} - \Delta\Gamma_S|^2 = 0. \tag{18}$$

Expansion and substitution of $|\Gamma_S| = 1$ into (18) results in (19), an equation for the intersections of the source stability circle and the unit circle

$$C_1\Gamma_S + C_1^*\Gamma_S^* - B_1 = 0. \tag{19}$$

Multiplying this equation by Γ_S and utilizing the quadratic formula gives two solutions

$$\Gamma_S^{\pm} = \frac{B_1 \pm \sqrt{B_1^2 - 4|C_1|^2}}{2C_1}.$$

From (6), (10), and, (11)

$$B_1^2 - 4|C_1|^2 = 4|S_{12}S_{21}|^2(k^2 - 1) \tag{20}$$

which implies that $|k| < 1$ is equivalent to $B_1^2 < 4\ |C_1|^2$. In this case the complex number $\Gamma_S^{\pm}$ is appropriately written

$$\Gamma_S^{\pm} = \frac{B_1 \pm j\sqrt{4|C_1|^2 - B_1^2}}{2C_1}. \tag{21}$$

The available power gain [5], G_A, is defined in terms of the normalized gain, g_a, as

$$G_A = g_a|S_{21}|^2 \tag{22}$$

where

$$g_a = \frac{(1 - |\Gamma_S|^2)}{|1 - S_{11}\Gamma_S|^2 - |S_{22} - \Delta\Gamma_S|^2}. \tag{23}$$

Contours of constant gain appear as circles [6] on the Smith Chart with centers and radii defined by

$$C_{\text{ga}} = c_{\text{ga}}\hat{c}_S$$
$$c_{\text{ga}} = \frac{|C_1|}{D_1 + \frac{1}{g_a}} \tag{24}$$

and

$$r_{\text{ga}} = \left|\frac{\left[1 - 2k|S_{12}S_{21}|g_a + |S_{12}S_{21}|^2 g_a^2\right]^{1/2}}{1 + g_a D_1}\right|. \tag{25}$$

The centers of the constant gain circles and the center of the stability circle all lie on a common ray drawn from the center of the Smith Chart defined by the unit vector $\hat{c}_S$.

Circles of constant available gain, g_a, are represented from (23) as

$$|1 - S_{11}\Gamma_S|^2 - |S_{22} - \Delta\Gamma_S|^2 = \frac{(1 - |\Gamma_S|^2)}{g_a}.$$

Substitution of $|\Gamma_S| = 1$, the unit circle, yields

$$|1 - S_{11}\Gamma_S|^2 - |S_{22} - \Delta\Gamma_S|^2 = 0$$

showing that the solution is independent of g_a, and hence the gain circle intersects the unit circle at the same point regardless of the gain, and consequently are referred to as *invariant points*. Also, this equation is the same as (18) implying that the invariant points are identical to points where the stability circle intersects the unit circle, i.e., $\Gamma_S^{\pm}$. Because of the invariant points, the geometric relationship of the source stability circle, gain circles and the unit circle can be determined solely by the center as shown in Fig. 3.

The behavior of the gain is now examined as one moves a distance x along the direction $\hat{c}_S$, i.e., letting $\Gamma_S = x\hat{c}_S$. Substitution into (23) yields

$$g_a(x) = \frac{1 - x^2}{D_1x^2 - 2|C_1|x + E_1}. \tag{26}$$

Differentiation of this expression yields

$$g_a' = \frac{2|C_1|x^2 - 2(D_1 + E_1)x + 2|C_1|}{(D_1x^2 - 2|C_1|x + E_1)^2}.$$

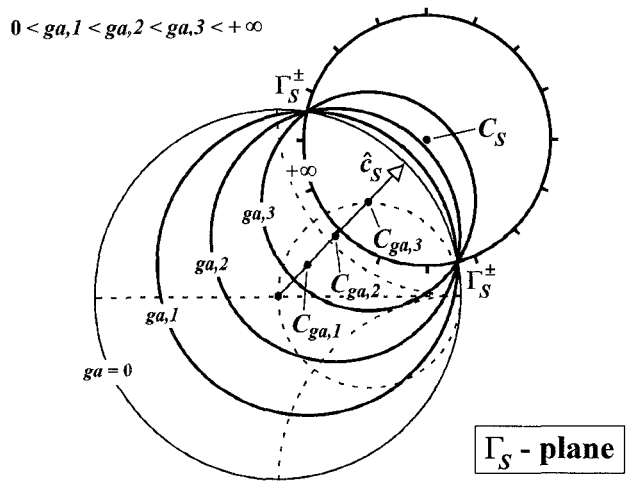

Fig. 3. Illustration of invariant points $\Gamma_S^{\pm}$ for a circuit where $|k| < 1$ and $D_1 > 0$.

Since the denominator is always positive the sign of the derivative is controlled by the numerator. The function, g_a, is monotonic (always increasing or always decreasing) when the numerator does not change sign as a function of x. This is equivalent to saying that the discriminant of the numerator, a quadratic, is negative, i.e.

$$4(D_1 + E_1)^2 - 16|C_1|^2 < 0$$

which is the same as (17), and therefore, equivalent to $|k| < 1$. Consequently, the gain function is a monotonic function of x whenever $|k| < 1$.

The gain function g_a in (23) is singular ($\pm\infty$) whenever Γ_S approaches a value on a stability curve since the denominator vanishes in (18). The sign of the singularity is determined by examine the numerator and denominator of (23). As long as Γ_S remains in the Unit Smith Chart the numerator is positive, and as long as Γ_S is in the stable region the denominator is positive. This positive monotonic nature of g_a is illustrated in Fig. 3 for $D_1 > 0$. The gain is zero at the boundary of the USC and approaches $+\infty$ as the stability circle is approached on the stable side, i.e., the "tick mark" side.

V. Input Stable Region in the Source Plane

The *input stable region in the source plane* is determined by $|\Gamma_{\text{IN}}(\Gamma^*_{\text{OUT}}(\Gamma_S))| < 1$. Substitution of (3) and (1) results in

$$|E_1 - C_1^*\Gamma_S^*| > |C_1 - D_1\Gamma_S^*|. \tag{27}$$

Squaring and expanding (27) results in

$$\begin{aligned}(|C_1|^2 - D_1^2)|\Gamma_S|^2 + (D_1 - E_1)C_1\Gamma_S \\ + (D_1 - E_1)C_1^*\Gamma_S^* > |C_1|^2 - E_1^2\end{aligned} \tag{28}$$

which describes a disk or disk complement region in the Γ_S-plane depending on whether $|C_1|^2 - D_1^2 < 0$ or $|C_1|^2 - D_1^2 > 0$, respectively. In either case the boundary of the region is described by the equation

$$\begin{aligned}(|C_1|^2 - D_1^2)|\Gamma_S|^2 + (D_1 - E_1)C_1\Gamma_S \\ + (D_1 - E_1)C_1^*\Gamma_S^* = |C_1|^2 - E_1^2\end{aligned} \tag{29}$$

which is a circle with center

$$C_{\text{IS}} = c_{\text{IS}}\hat{c}_S$$

where

$$c_{\text{IS}} = \frac{|C_1|}{D_1 + \frac{|S_{12}S_{21}|}{2k}} \tag{30a}$$

and with radius

$$r_{\text{IS}} = \left|\frac{|S_{12}S_{21}|}{2kD_1 + |S_{12}S_{21}|}\right|. \tag{30b}$$

The subscript "IS" signifies that the area of interest is the Input stability region in the Source plane.

Noticing that C_{IS} is co-linear with the centers of the available gain circles, C_{ga}, (line determined by the unit vector $\hat{c}_S$) motivates an examination of whether the input stable circle intersects the unit circle. Substitution of $|\Gamma_S| = 1$ into (29) results in (19) and shows that the input stable circle in the source plane intersects the unit circle at exactly the invariant points and hence *the input stable boundary in the source plane is an available gain circle* [7].

The specific gain value equating to the input stable boundary is denoted g_{is} signifying that it is the specific available gain circle which determines the input stable region in the source plane. The value of g_{is} can be found by equating (24) with (30a) resulting in

$$g_{\text{is}} = \frac{2k}{|S_{12}S_{21}|}.$$

The denormalized gain equals

$$G_{\text{IS}} = 2 \cdot k \cdot \left|\frac{S_{21}}{S_{12}}\right| = 2 \cdot k \cdot \text{MSG}$$

where MSG is the maximum stable gain of the device.

The g_{is} available gain circle determines the boundary for the input stable region in the source plane, i.e. $|\Gamma_{\text{IN}}(\Gamma^*_{\text{OUT}}(\Gamma_S))| < 1$. However, it remains to determine when and if g_{is} represents an upper bound for the available gain.

VI. Maximum Available Gain (For Passive Jointly Stable Source Impedances)

In this section it is shown that when the source impedance is required to be passive and *jointly input/output stable* then the available gain has an upper bound referred to as the maximum jointly stable available gain. This requires examining the geometrical relationship of the g_{is} circle (input stable region boundary in the source plane), the unit circle ($|\Gamma_S| = 1$), the

TABLE I
COMBINATION OF STABILITY REGIONS IN THE Γ_S-PLANE FOR $|k| < 1$

Case	Output Stable Region (D_1)	Input Stable Region ($\lvert C_1\rvert^2 - D_1^2$)	Implied k values	Implied Relationship of centers	Fig #	Does Passive Jointly Stable Region Exist?
I	Outside (>0)	Outside (>0)	$k>0$	$0<c_{IS}<c_S$	4	Yes
			$k\le 0$	$c_{IS}\le 0<c_S$	5	No
II	Outside (>0)	Inside (<0)	$k<0$	$0<c_S<c_{IS}$	6	No
III	Inside (<0)	Inside (<0)	$k>0$	$c_{IS}<c_S<0$	7	Yes
IV	Inside (<0)	Outside (>0)	$k>0$	$c_S<0<c_{IS}$	8	Yes
			$k\le 0$	$c_S<c_{IS}\le 0$	9	No

source stability circle (output stable region boundary in the source plane) and the resulting implication of the monotonic and singular nature of the gain. The geometry of the circles is determined by the centers since they all intersect at the invariant points. The passive, output stable, and input stable regions in the *source plane* are

Passive Source region $[|\Gamma_S| < 1]$

Output Stable region $[|\Gamma_{\mathrm{OUT}}(\Gamma_S)| < 1]$

$D_1 > 0$: stable region is outside the source stability circle
$D_1 < 0$: stable region is inside the source stability circle

Input Stable region $[|\Gamma_{\mathrm{IN}}(\Gamma^*_{\mathrm{OUT}}(\Gamma_S))| < 1]$

$|C_1|^2 - D_1^2 > 0$: stable region is outside the g_{is} circle
$|C_1|^2 - D_1^2 < 0$: stable region is inside the g_{is} circle.

Combinations of the possible stable regions above results in four cases to consider. Case I is analyzed in detail below, while the remaining cases are summarized in Table I.

Case I: $D_1 > 0$ and $|C_1|^2 - D_1^2 > 0$.

Substitution of (10) and (11) results in

$$|C_1|^2 - D_1^2 = |S_{12}S_{21}|(|S_{12}S_{21}| + 2kD_1) > 0$$

which implies that

$$k > -\frac{|S_{12}S_{21}|}{2D_1}.$$

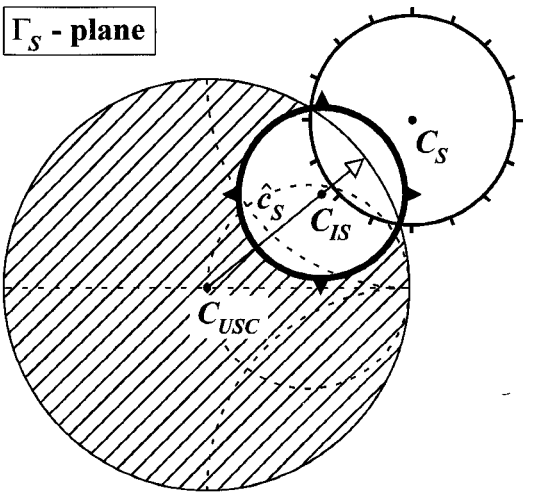

Fig. 4. Case I geometry ($D_1 > 0$ and $|C_1|^2 - D_1^2 > 0$) when $0 < k < 1$ implies $0 < c_{\mathrm{IS}} < c_S$.

If k is positive then

$$0 < \frac{|C_1|}{D_1 + \frac{|S_{12}S_{21}|}{2k}} < \frac{|C_1|}{D_1}$$

and from (13) and (30a)

$$0 < c_{\mathrm{IS}} < c_S$$

which shows the relationship of the scalar multipliers used with the unit vector $\hat{c}_S$ to determine the centers of the circles. This is illustrated in Fig. 4 where the stable side of the source stability circle is indicated by tick marks. The input stability boundary (g_{is}) in the source plane is illustrated as a dark circle with the stable side designated by triangular tabs. The shaded area shows the passive, jointly stable impedances in the source plane (drawing conventions apply to all figures in this section). Since $D_1 > 0$ the available gain function is increasing as Γ_S moves along the line defined by the vector $\hat{c}_S$. From the discussion connected with Fig. 3, the gain equals zero when Γ_S is located at the boundary of the USC and goes to $+\infty$ as it approaches the stability circle on the tick mark side. Therefore, in this case with $k > 0$, the available gain for passive, jointly stable source impedances is bounded by G_{IS}.

When $k = 0$, the input stable boundary in the source plane becomes the same as the unit circle as can be seen by taking the limit as k approaches zero in (30a) and (30b). However, the input stable region is outside the circle and therefore it is impossible to have a passive source impedance which is also jointly stable.

When $k < 0$ then $0 < c_{\mathrm{IS}} < c_S$ and no passive jointly stable source impedances are possible as illustrated in Fig. 5.

After all possible topological combinations of passive and jointly stable regions in the source plane have been similarly examined (see Table I) and it is observed that when $0 < k < 1$ then the jointly stable region overlaps with the USC. Source impedances in the overlapping region result in an output whose conjugate match is located on the stable side of the load stability circle. The available gain value, G_{IS}, represents an upper bound for passive, jointly stable source impedances. When $-1 < k \le 0$ no passive source impedance are possible

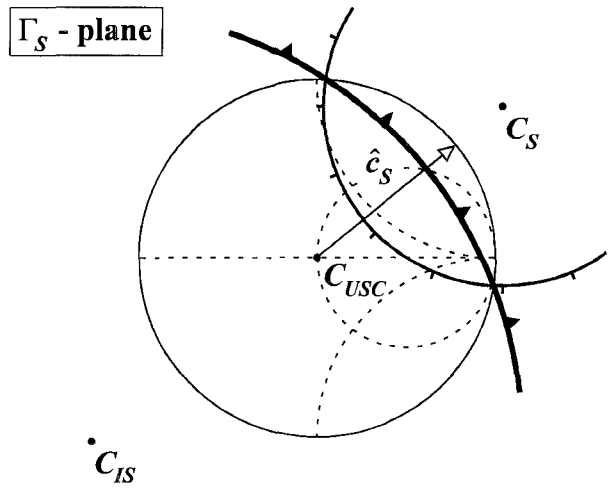

Fig. 5. Case I geometry ($D_1 > 0$ and $|C_1|^2 - D_1^2 > 0$) when $-1 < k \leq 0$ implies $c_{IS} \leq 0 < c_S$.

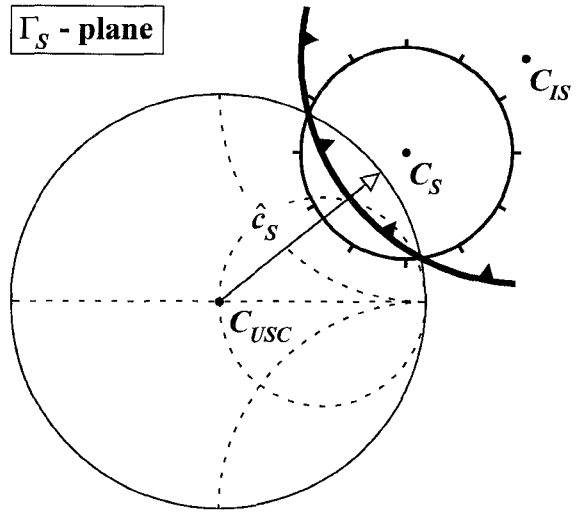

Fig. 6. Case II geometry ($D_1 > 0$ and $|C_1|^2 - D_1^2 < 0$) implies $-1 < k < 0$ and $0 < c_S < c_{IS}$.

that are jointly stable in the source plane. Therefore, provided that $0 < k < 1$ the maximum available gain for jointly stable source impedances equals $G_{IS} = 2{\cdot}k{\cdot}$ MSG.

VII. Maximum Operating Gain (For Passive Jointly Stable Load Impedances)

The above development has concentrated on conditionally stable circuits with the output conjugately matched and $|k| < 1$. Similarly, a conditionally stable circuit can be designed with the input conjugately matched. In this case the load impedance determines whether the circuit is input stable

$$|\Gamma_{IN}(\Gamma_L)| < 1$$

or output stable,

$$|\Gamma_{OUT}(\Gamma_{IN}^*(\Gamma_L))| < 1.$$

In this case analogous definitions and relationships for (6) through (13) exist and can be used to establish that output

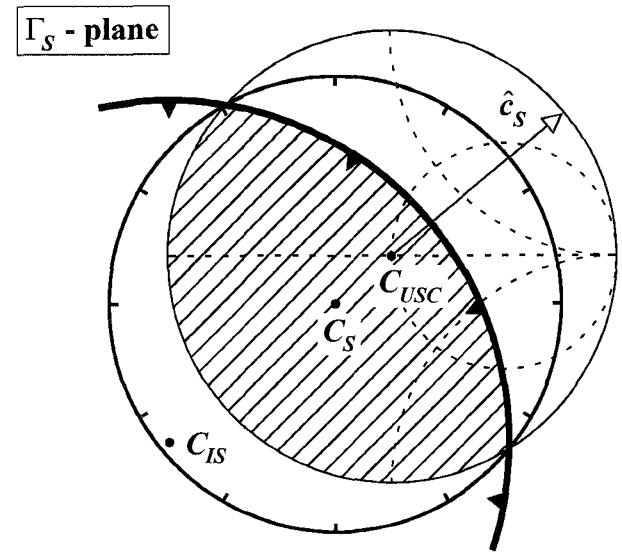

Fig. 7. Case III geometry ($D_1 < 0$ and $|C_1|^2 - D_1^2 < 0$) implies $0 < k < 1$ and $c_{IS} < c_S < 0$.

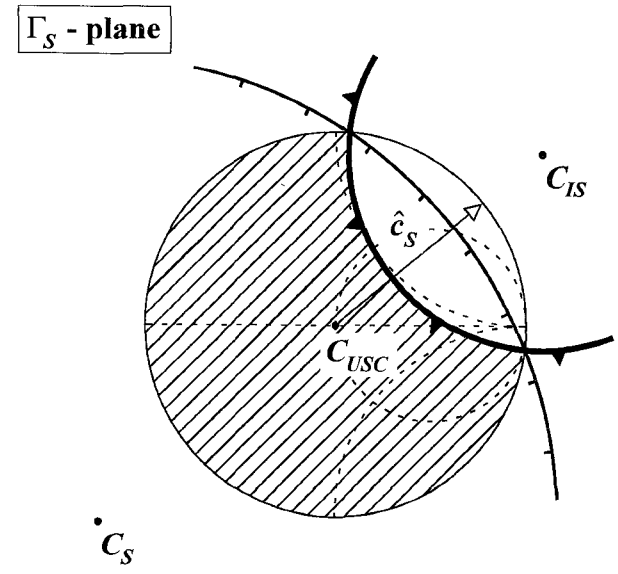

Fig. 8. Case IV geometry ($D_1 < 0$ and $|C_1|^2 - D_1^2 > 0$) when $0 < k < 1$ implies $c_S < 0 < c_{IS}$.

stable region in the load plane is bounded by an operating gain circle with center $C_{OL} = c_{OL}\hat{c}_L$ where

$$c_{OL} = \frac{|C_2|}{D_2 + \frac{|S_{12}S_{21}|}{2k}}$$

$$\hat{c}_L = \frac{C_2^*}{C_2}$$

and radius

$$r_{OL} = \left| \frac{|S_{12}S_{21}|}{2kD_2 + |S_{12}S_{21}|} \right|.$$

The output stable region in the load plane is inside the circle if $|C_2|^2 - D_2^2 < 0$ if and outside if $|C_2|^2 - D_2^2 > 0$. The value of the normalized gain is

$$g_{ol} = \frac{2k}{|S_{12}S_{21}|}$$

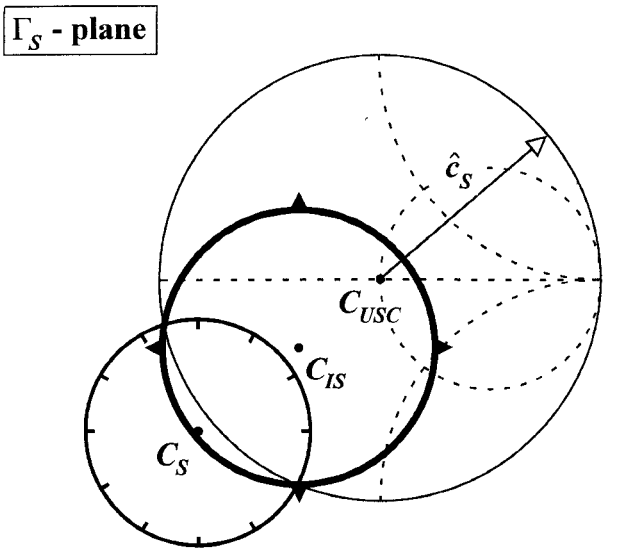

Fig. 9. Case IV geometry ($D_1 < 0$ and $|C_1|^2 - D_1^2 > 0$) when $-1 < k \leq 0$ implies $c_S < c_{IS} \leq 0$.

with an denormalized gain equal to

$$G_{OL} = g_{ol}|S_{21}|^2 = 2 \cdot k \cdot MSG.$$

It also follows that passive, jointly stable load impedances exist if and only if $0 < k < 1$ and the operating gain is bounded by G_{OL}.

VIII. Maximum Single-Sided Matched Gain (For Passive Jointly Stable Impedances)

Since the maximum available gain for passive, jointly stable source impedances equals the maximum operating gain for passive, jointly stable load impedances, a universal figure of merit can be defined and designated as Maximum Single-Sided Matched Gain, G_{MSM}, for conditionally stable amplifier. And, for which

$$G_{MSM} = G_{IS} = G_{OL} = 2 \cdot k \cdot \text{MSG}.$$

In particular, $G_{MSM} > G_{MSG}$ if $k > \frac{1}{2}$.

IX. Design Example

This section illustrates the use of the above principles in the design of a conditionally stable 6 GHz amplifier using the Mitsubishi MGF-4301A HEMT with a conjugately matched output. The design is based on measured S-parameters for 37 devices biased at $V_{DS} = 2$ V, $I_{DS} = 20$ mA and summarized in Table II. Using the mean values from Table II one finds that $\bar{k} = .732$, $\bar{G}_{MSG} = 17.2$ dB, and $\bar{G}_{MSM} = 18.9$ dB.

The design begins by selecting a source stability margin measured by an acceptable reduction of available gain. For each device, an input matching point is selected to insure that the available gain is 2 dB below its G_{MSM}. This point is determined for each transistor by selecting Γ_S on the line connecting the center of the Smith Chart and the gain circles so that each Γ_S is at a maximum distance from their respective MSM circles. The Γ_S for a desired available gain can be found

TABLE II
Statistical Summary for S-Parameters Measurement of 37 Mitsubishi MGF-4301A MESFET's, at 6 GHz

MGF-4301 A	Average		Standard Deviation	
	Real Part	Imag Part	Real Part	Imag Part
S_{11}	- 406	- 554	016	017
S_{21}	1.45	3.93	.089	.098
S_{12}	076	021	003	001
S_{22}	092	- 409	021	008

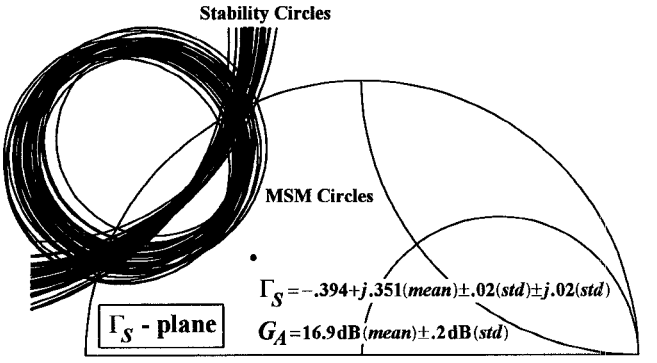

Fig. 10. Source stability circles, MSM circles, and the average input matching point for the 37 transistors at 6 GHz.

by inverting (26) using the negative root in the quadratic formula

$$x = \frac{|C_1|g_a - \sqrt{|C_1|^2 g_a^2 - (g_a D_1 + 1)(g_a E_1 - 1)}}{(g_a D_1 + 1)}$$

and substituting into

$$\Gamma_S = x \cdot \hat{c}_S$$

where g_a from (22) now equates to the reduced gain for each device.

The average of the 37 Γ_S's together with the source stability circles, and the MSM circles, calculated using (12a), (12b), (24), (25), (30a), and (30b) are shown in Fig. 10. A single IMN matched to the average Γ_S was designed using the HP-EEsof commercial CAD system.

A set of output reflection coefficients is subsequently obtained by connecting the same IMN to each of the transistors. Averaging the conjugate of this set determines the matched load reflection coefficient, see Fig. 11, and is used to design the OMN.

With the IMN and OMN designed, transducer gain of the amplifier can be simulated using the S-parameters of each device. A plot of these transducer gains is shown over a frequency range of 4–8 GHz in Fig. 12. The black band resulting from multiple traces indicates the variation of gain over the 37 samples. The average transducer gain at the 6 GHz design frequency is 16.7 dB (mean) ±0.2 (std).

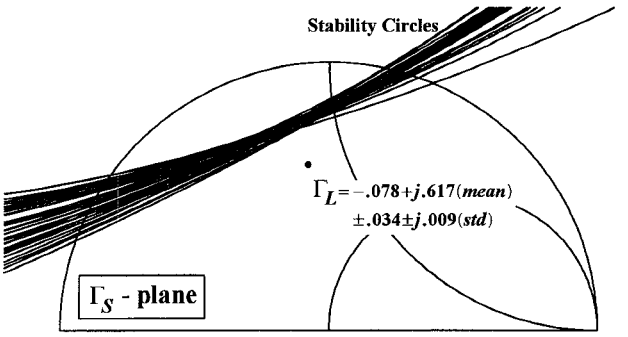

Fig. 11. Load stability circles and the average conjugately matched load for the 37 transistors at 6 GHz.

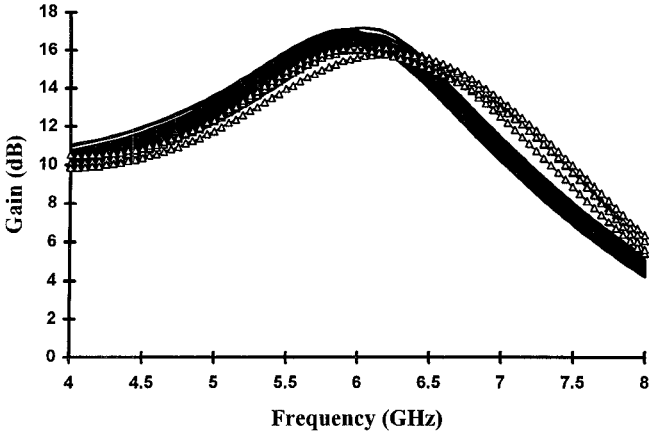

Fig. 12. Simulated and measured (Δ) gain for an output matched conditionally stable amplifier using the Mitsubishi MGF-4301A transistors.

The above design was fabricated and transistors installed. The measured gain of four output matched amplifiers are shown in Fig. 12. The average gain of the four amplifiers measured at 6 GHz is 15.9 dB.

The advantage of pursuing a conditionally stable design technique is illustrated by comparison with the expected performance of an unconditionally stable amplifier design using the same transistor set. The expected MAG can be estimated as MSG − 2.7 − .5 = 14.0 dB, where the 2.7 dB reduction accounts for resistive loading to achieve $k \approx 1.2$ and the .5 dB reduction accounts for typical matching network losses. A design k of 1.2 was assumed here to provide design margin so that actual circuit k's will be maintained greater than one under worst-case component and process variations. On the basis of similar design margins and circuit losses, the 6.7 dB gain of the conditionally stable design is 2.7 dB higher than the 14-dB gain of the unconditionally stable design. Even the measured gain of the conditionally stable amplifier design (Fig. 12) is nearly 2 dB better than the design estimate of the unconditionally stable amplifier. This improvement is achieved without the side effects of resistive loading such as increased noise figure.

The gain improvement was possible because some instability risk was permitted to be part of the design. A quantitative margin of safety is, therefore, important and must be considered for a wide frequency range even in a narrow band design. Plotting the circuit k and B_1 values as a function

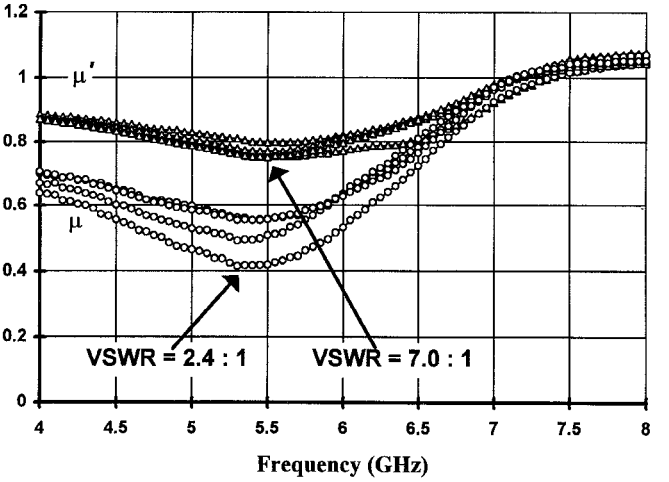

Fig. 13. Stability margin determined by μ' and μ.

of frequency is not very satisfying since it does not directly translate into VSWR restrictions on the source or load to insure stable operation. However, the new source and load stability parameter μ' and μ [3] which measures the encroachment of the unstable area onto the USC does provide the necessary source and load VSWR condition. Fig. 13 shows μ' and μ plotted for the four fabricated amplifiers over a frequency range of 4–8 GHz. The stability margin is determined on the source side by μ' and on the load side by μ. The lowest values determine the least margin of stability. For example at 5.5 GHz $\mu' = 0.75$ which equates to a VSWR of (1+.75)/(1−.75) = 7.0 meaning that the circuit remains stable even when connected to a source having a high VSWR of 7.0:1. At 5.3 GHz $\mu =$ 0.42 implies that stable operation is insured for a load whose VSWR does not exceed 2.4:1.

The above techniques naturally lend themselves to modern, commercially available CAD packages which easily incorporate user defined variables and equations and the relationships can greatly accelerate optimization and provide valuable engineering insight into the design.

X. Conclusion

A deterministic approach has been developed for designing conditionally stable amplifiers whose input or output is matched. A rigorous theoretical framework for this approach has been established and two gain circles have been defined, namely the Maximum Available Gain for passive, jointly stable source impedances and the Maximum Operating Gain for passive, jointly stable load impedances. Each circle serves as a graphical design aid on the Smith Chart as the boundary for suitable source or load regions under the proposed design method. The boundary of both regions coincides with a particular gain circle in their respective impedance plane and the associated gain of each circle is found to be equal to $2 \cdot k \cdot$ MSG. This gain is designated as G_{MSM} (Maximum Single-sided Matched Gain).

References

[1] M. W. Medley, *Microwave and RF Circuits: Analysis, Synthesis and Design.* Norwood, MA: Artech House, 1993, pp. 106 and 111.

[2] G. Gonzalez, *Microwave Transistor Amplifiers*. Englewood Cliffs, NJ: Prentice-Hall, 1984, pp. 92–102.
[3] M. L. Edwards and J. H. Sinsky, "A new criterion for linear 2-port stability using a single geometrically derived parameter," *IEEE Trans. Microwave Theory Tech.*, vol. 40, no. 12, pp. 2303–2311, Dec. 1992. This reference discussed the load stability circle and the conditions on D_2 which naturally translate to the source stability circle and D_1 conditions mentioned in this paper.
[4] R. E. Collins, *Foundations for Microwave Engineering*, 2nd ed. New York: McGraw Hill, 1992, pp. 716, 725–726, and 750–759.
[5] G. D. Vendelin, A. M. Pavio, and U. L. Rohde, *Microwave Circuit Design Using Linear and Nonlinear Techniques*. New York: Wiley, 1990, p. 59.
[6] H. Fukui, "Available power gain, noise figure, and noise measure of two-ports and their graphical representation," *IEEE Trans. Circuit Theory*, vol. CT-13, no. 2, pp. 137–142, June 1966.
[7] J. H. Sinsky, "Selected topics in stability and gain for active 2-port networks," Spec. Proj. Rep., G. W. C. Whiting School of Engineering, Johns Hopkins University, May 1992.

Marion Lee Edwards (S'61-M'79-SM'84) received the B.S. and M.S. degrees in electrical engineering from N.C. State University and Northwestern University, respectively and the Ph.D. degree in mathematics from the University of Maryland.

He has joint appointments at the Johns Hopkins University. He is the supervisor of the Microwave and RF Systems group in the Space Department of the Applied Physics Laboratory and is the Electrical Engineering Program Chair in the G.W.C. Whiting School of Engineering. He has been a leader in both the R&D and educational aspects of microwave development at Johns Hopkins. As the J. H. Fitzgerald-Dunning Professor he assisted in the development of the Hopkins undergraduate microwave laboratory program. He has experience in the design of microwave integrated circuits (MIC) and monolithic microwave integrated circuits (MMIC) and has a continuing interest in the modeling of circuits suitable for the development of a microwave library based methodology.

Dr. Edwards is a member of Eta Kappa Nu, Tau Beta Pi, Pi Mu Epsilon, Phi Kappa Phi, and Sigma Xi.

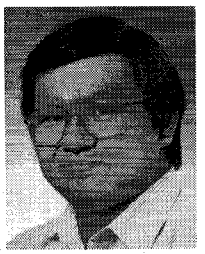

Sheng Cheng (M'88) was born in Taipei, Taiwan in 1959. He received the B.S. and M.S. degrees in electrical engineering from the National Taiwan University and Johns Hopkins University in 1982 and 1989, respectively.

Since August of 1990 he has been employed as a Senior Development Engineer with the G.W.C. Whiting School of Engineering, Johns Hopkins University. He currently manages the Whiting School microwave engineering research facilities at the Dorsey Center where he works closely with government and industry sponsors such as Army Research Laboratory, HP/HP-EEsof, Cascade Microtech, Rogers Corp, and etc. He has been involved in the research and education of microwave circuit theory, design methodology and testing. His experience includes both MIC and MMIC designs and measurements.

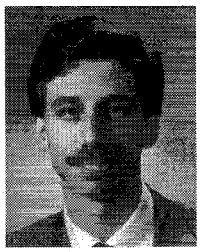

Jeffrey H. Sinsky (S'83-M'85) was born in Baltimore, MD in 1963. He received the B.Sc. and M.Sc. degrees in electrical engineering from The Johns Hopkins University in 1985 and 1992 respectively, and is currently pursuing the Ph.D. at The Johns Hopkins University in the Electrical and Computer Engineering Department.

Since June of 1985 he has been employed at the Johns Hopkins University Applied Physics Laboratory. He is currently a Senior Engineer in the Space Department. His work experience has included development of real-time missile tracking software, design and specification of microwave flight hardware, microstrip antenna design, and research in the area of power GaAs MMIC design. His interests include microwave circuit design, microwave theory, and satellite communication systems design.

Mr. Sinsky was the recipient of the John Boswell Whitehead award for outstanding achievement in electrical engineering and computer science by an undergraduate student and was also a finalist in the Alton B. Zerby Award competition for the outstanding electrical engineering student in the USA in 1985. He is a member of Tau Beta Pi and a member/past chapter president of Eta Kappa Nu.